JOURNAL OF MATERIALS SCIENCE 23 (1988) 1580–1590

A fracture mechanics approach to the effects of UV-degradation on polypropylene

G. E. SCHOOLENBERG
Department of Industrial Design Engineering, Technical University of Delft, Oude Delft 39a, 2611 BB Delft, The Netherlands

A fracture mechanics approach to the ultraviolet-degradation embrittlement of polypropylene (PP) semi-crystalline homopolymer has been evaluated. The loss in fracture properties results mainly from embrittlement of the surface, resulting in surface defects. Hence, the fracture energies of degraded and single edge notched (SEN) specimens were compared to test to what extend they agree. PP specimens were degraded artificially in a Xenontest. Degradation depth was measured by Fourier transformed infrared (FTIR) spectrometry. Degraded and notched specimens were tested at different deformation velocities in three-point bending. Fracture energies of degraded specimens and specimens notched with a depth equal to that of degradation were compared. Differences were accounted for by different fracture processes which were observed by studying fracture surfaces.

1. Introduction

Many polymers are embrittled when they are irradiated by ultraviolet light. The result is that plastic products which have been exposed to outdoor conditions fracture easily, especially on impact. Usually the embrittlement is caused by the breaking of chemical bonds and subsequent reactions with oxygen, which lowers the molecular weight [1, 2].

In general, the loss in fracture properties by ultraviolet degradation is characterized by the so-called "half-time". This is the degradation time after which a 50% decrease of some property is observed. Very often the property tested is the loss of elongation to break in a slow tensile test.

Although this method gives information on the lifetime of the material, and is useful when following the degradation process in time, it does not state the loadability of a plastic product. The loadability of an ultraviolet-degraded product (or test specimen) proves to be dependent on product size and geometry, load direction [3] and deformation rate.

Usually reduction of the elongation to break at low deformation rates is not the most important limitation for use, as long as the yield point is not affected. At higher deformation rates (impact) the transition from ductile to brittle behaviour causes severe loss of fracture energy which is the principal concern of the user.

When a degraded polymer is analysed chemically, it is usually found that only a very thin surface layer is affected. In the PP homopolymer we used in our investigation this layer was 500 μm thick at the utmost. The material underneath had not changed chemically.

However, this layer can still cause a severe loss of fracture resistance, because it fractures at low loads or even spontaneously during the degradation process. The result is a surface defect, from which final fracture appears easily (e.g. [4–8]). The strength of a product with a flaw or defect can be calculated by fracture mechanics. It is necessary to determine the size of the defect, the fracture resistance of the material and the influence of the geometry.

Crack propagation occurs if $K > K_c$ or $G > G_c$ by the well-known equations

$$K = pYa^{1/2} \quad (1)$$

or in energy terms

$$G = K^2/E' \quad (2)$$

where K is stress intensity, p is stress, a is crack length, G is energy release rate and E' is Young's modulus, E, for plane stress conditions, and for plane strain E' is $E/(1 - \nu)$, where ν is Poisson's ratio. Y is a geometrical factor which, if known, enables the prediction of the residual strength of a part, if the material constants K_c or G_c are known as well.

In case the loss of fracture energy of ultraviolet-degraded polymers is actually caused by a surface defect in the embrittled layer, the fracture process is similar to that of a non-degraded material with a crack or notch. This led to the hypothesis that the loadability of a polymer product could be calculated if the crack size, i.e. the depth of the embrittlement, is known. Because geometry factors in fracture mechanics are known for many geometries and loading conditions, this opens possibilities to predict the loadability of a degraded plastic product.

The following sections describe the research we performed in order to test the validity of this approach. This research consisted of determining the fracture energy of degraded specimens, the depth of embrittlement, and the fracture energy of specimens with notches of the same depth.

0022–2461/88 $03.00 + .12

2. Experimental details

2.1. Test specimens

Of the two PP materials used, one was not stabilized against ultraviolet radiation (material N) and the other contained an ultraviolet absorber (material S). To avoid shear stresses and morphology transitions as much as possible, specimens were cut from compression moulded plates, which were cooled down slowly ($30°\,C\,min^{-1}$). This resulted in equally sized spherulites of $\sim 100\,\mu m$, while skin–core morphology transitions were absent. The specimens measured 4 mm × 4 mm × 50 mm. They were degraded in a Xenontest 1200 weather simulation machine of Original Hanau (operated at 40° C). For PP films, 100 h was stated to be equivalent to ~2 months exposure outdoors, in western Europe conditions (averaging both climatical and seasonal variations) [9]. N.B. The non-stabilized material was not designed to be used outdoors.

2.2. Notching

A group of specimens was degraded; another group was notched with a razor blade. The razor blade was clamped between two blocks and placed on the specimen. A dead weight was dropped on the clamps to drive the razor blade into the specimen. This made it possible to produce sharp, very short notches, comparable to those that originate from the cracking of the embrittled layer.

2.3. Measurement of the thickness of the degraded layer

The thickness of the degraded layer of the exposed specimens was measured in several ways. After some time the degraded specimen shows a pattern of fine cracks on its surface which grows spontaneously during exposure and develops further during the fracture process. The depth of these cracks can be measured by microtoming thin slices from the surface, and examining them, as described later. The slices were also examined by FTIR spectrometry and the carbonyl index (1720 over $1254\,cm^{-1}$) was measured. In this way a profile of the oxidation through the depth could be established.

2.4. Three-point bending test

The specimens were tested in three-point bending. The three-point bending test consists of an instrumented tup, mounted on a servo-hydraulic actuator. The actuator can produce tup rates of 10^{-3} up to $3.5\,m\,sec^{-1}$. The force is registered by a piezo-element. The displacement is measured by a linear variable displacement transducer (LVDT) and controlled by a servo-valve, in order to be linear in time. In our investigation we selected tup rates from 10^{-2} up to $2.5\,m\,sec^{-1}$. Specimens were tested with the degraded or notched sides in the tension side of the specimen.

2.5. Microscopy

Fracture surfaces were gold-coated and inspected in a scanning electron microscope (SEM). Thin slices from the embrittled surface were analysed using polarized light microscopy.

3. Test results

3.1. Fracture energy of degraded specimens

Figs 1 and 2 show the specific fracture energy (energy per fractured area) of non-stabilized (N) and stabilized (S) material, respectively, at two different tup rates. At $1.5\,m\,sec^{-1}$ a serious reduction of the fracture energy is observed for both materials.

The half time of the specific fracture energy is extended from 150 h to about 250 h by stabilization. Material N gives a very low specific fracture energy at 250 h, after which an increase is observed. Material S does not reach this very low level.

At $0.01\,m\,sec^{-1}$ material N shows a decrease in specific fracture energy at 150 h as well, which is the half time at $1.5\,m\,sec^{-1}$. However, at zero and very short exposure times, the specimens are deformed to such extremes that they are pushed through the fixtures of the anvil without fracture and no actual fracture energy could be measured at this speed. Material S shows the same behaviour at $0.01\,m\,sec^{-1}$, but the reduction of the specific fracture energy is smaller.

3.2. Condition of the embrittled surface

Visual inspection of the specimens before and after fracture showed surface conditions as in Fig. 3.

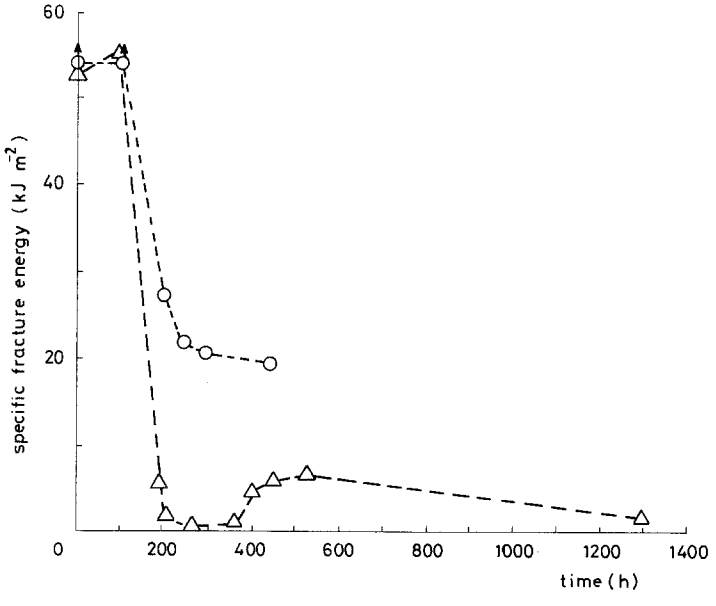

Figure 1 Specific fracture energy plotted against radiation time of non-stabilized (N) material; data points are the averages of seven specimens. Tup rates: (△), 1.5 and (○) $0.01\,m\,sec^{-1}$. Unbroken specimens are indicated with a vertical arrow.

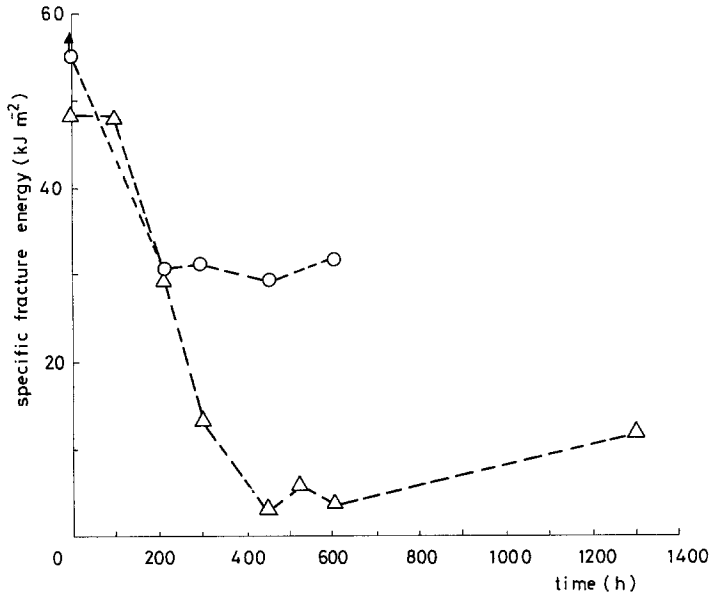

Figure 2 Specific fracture energy plotted against exposure time of stabilized (S) material. Tup rates: (△) 1.5 and (○) 0.01 m sec^{-1}.

Between 250 and 300 h cracks become visible in the surface. At 1300 h (not shown in Fig. 3) the surface is completely crumbled and powdery. The surface conditions differ from those reported by Qayyum and White [10], where no damage or only small fissures were observed. They used injection moulded specimens, whereas those investigated here were compression moulded.

This is probably the reason for the difference. At present a study on injection moulded specimens of the same material is being performed, where again we observe only small fissures. We hope to report this study in future.

After fracture the surface damage is increased. The specimens degraded for 100 h showed crazes. These were similar to those which occurred in fractured specimens that were neither notched nor degraded. At 150 h very fine cracks were visible. After longer exposure times, e.g. 200 to 250 h, the fractured specimens showed clear cracks, mostly perpendicular to the stress direction (see Figs 3c, d and e.) The closer to the fracture, the more cracks are formed. At 300 h, near the fracture the pattern is densified and new cracks have grown preferably in the direction perpendicular to stress, but other directions were also observed (Figs 3f and g). Finally, at 450 h, the surface was completely cracked even before fracture (Fig. 3h), while afterwards the cracks broadened and increased in number (Fig. 3i).

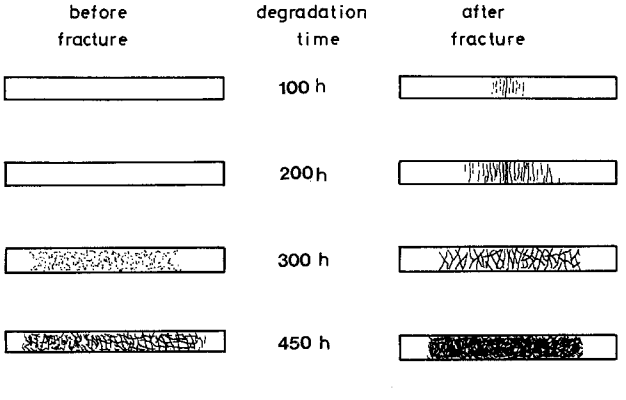

(a)

Figure 3 (a) Surface conditions of degraded specimens of material N. Left: after degradation, right after degradation and fracture at 1.5 m sec^{-1} (broken halves were fitted together). (b to i) Scanning electron micrographs of degraded surface; direction of tensile stress is horizontal for all pictures, slender black arrows indicate cracks. (b) Undegraded surface, before fracture; (c) degraded for 200 h, after fracture; (d) degraded for 250 h, after fracture, area close to the fracture (diagonal grooves are mould marks); (e) as (d) area remote from the fracture; (f) degraded for 300 h, after fracture; (g) degraded for 300 h, after fracture; (h) degraded for 450 h, before fracture; (i) degraded for 450 h, after fracture.

We now consider the fracture energies together with the surface conditions in Fig. 3. The very low fracture energies at 200 to 300 h that appear in Fig. 1, are not caused by surface cracks before fracture. The embrittled surface is cracked during the fracture process. This gives an even lower fracture energy than when surface cracks, grown spontaneously during degradation, are present before fracture (e.g. after 450 h).

3.3. Degradation depth

To be able to compare the degraded specimens with notched specimens, the degradation depth had to be determined. The degradation depth was measured by taking FTIR spectra of 15 μm thick slices, cut from the surface. The carbonyl index of these slices was plotted against the average depth from which they were taken. Through these data an exponential curve was fitted (Fig. 4). After 450 h it was observed that for the non-stabilized material, the carbonyl index levels off at the surface, which was also reported by Cunliffe and Davis [11].

Apart from the carbonyl (C = O) index, the depth of the cracks in Fig. 3 (after fracture) was also measured. At degradation times shorter than 250 h, all cracks are perpendicular to the stress direction. At longer times, the surface was cracked spontaneously, and these cracks were randomly orientated. However, the pattern changed with depth from randomly orientated cracks, to cracks perpendicular to the stress direction as well. Obviously the latter cracks form during the fracture process but are arrested either by unloading or because there is a change in fracture resistance.

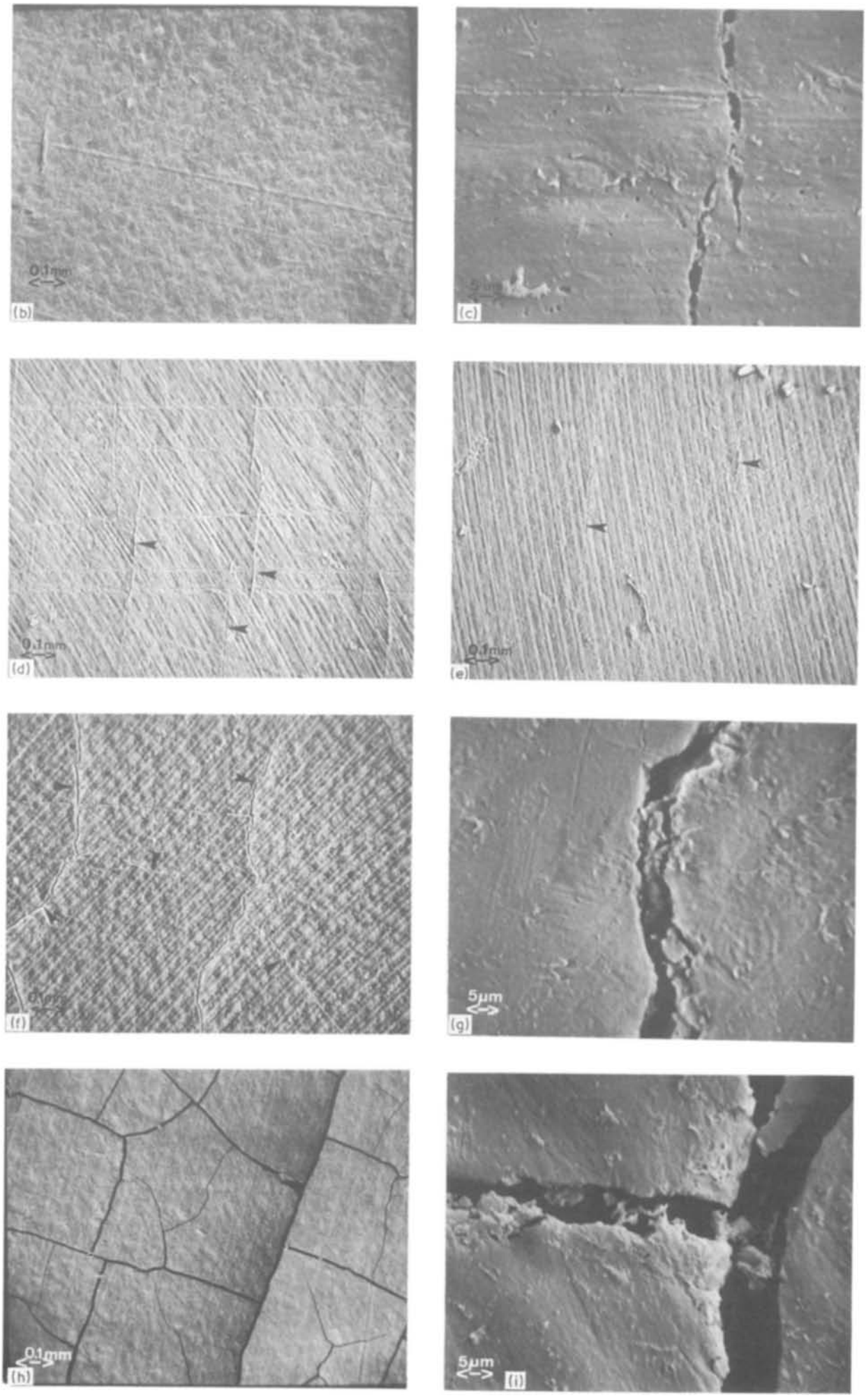

Figure 3 Continued.

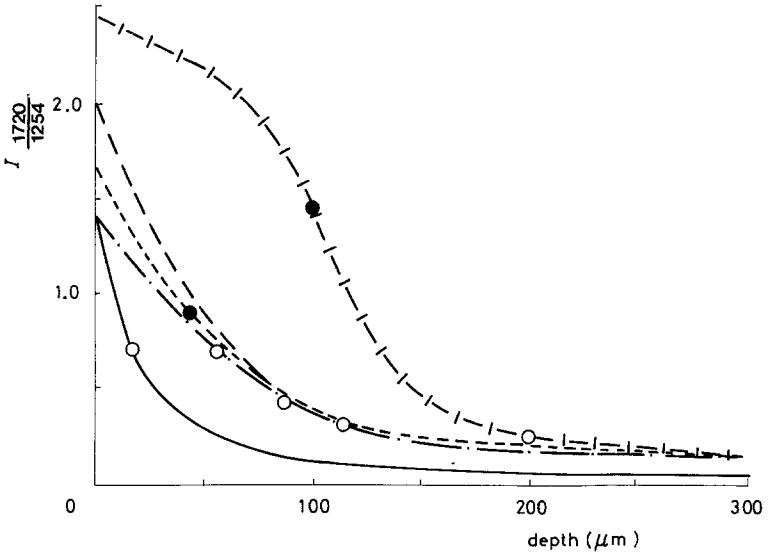

Figure 4 Carbonyl index of non-stabilized (N) material at several degradation times. (○) a_i = crack length of cracks perpendicular to stress, (●) a_0 = length of randomly orientated cracks spontaneously formed during degradation. (——) 100 h, (—·—) 200 h, (— —) 250 h (- - -) 300 h, (-|-) 450 h.

Both the depth of the spontaneous cracks (a_0) and the point of crack arrest (a_i) were measured as illustrated in Fig. 5. Transitions in crack patterns were detected by microscopic inspection of the slices. In the specimens degraded for 250 h or more, the crack arrest point was close to where the C=O level stabilizes (Fig. 4). At shorter degradation times, crack arrest occurs in material with a higher C=O level. The depth of the embrittlement was assumed to be the depth at which the C=O index approaches its asymptotic value. This is an arbitrary choice because the relation between the C=O index and the embrittlement of the material is unknown, and the measurement of the crack arrest point has not given consistent results compared to the C=O index so far. The assumption seems to be conservative and it may be expected that the fracture energy of specimens, with a notch size equal to this depth, is lower than that of the degraded specimens.

4. Comparison of results and discussion

The fracture energy of notched specimens was measured at the same tup rates as selected for the degraded specimens. The data were analysed by the methods proposed by Plati and Williams [12], to determine G_c. The G_c values proved to be reasonably constant within the range of crack lengths of interest. This enabled us to calculate fracture energies for all crack lengths required.

In Figs 6 and 8 the results of notched specimen data are plotted over the data in Figs 1 and 2. The notch sizes at all degradation times are equal to the depth of embrittlement as described previously (some values were obtained by interpolation).

At 1.5 m sec^{-1} the specific fracture energy in Fig. 6 at 200 to 400 h is much lower for the degraded specimens, than for the notched specimens. This suggests that fracture is not just caused by surface defects. Before introducing other theories, it was checked whether the notches were made sharp enough. This involved notching the specimen at −50° C and precracking by fatigue. None of this produced significant reductions of the fracture resistance. The fracture resistance we did find, corresponds well to data given by Sandt [13] and Casiraghi and Savadori [14].

The values at 0.01 m sec^{-1} match the notched data better, but underestimate specific fracture energy after longer times.

Fig. 7 shows the effect of deformation rate on the specific fracture energy of a series of specimens degraded 250 h, and specimens with a notch. At low

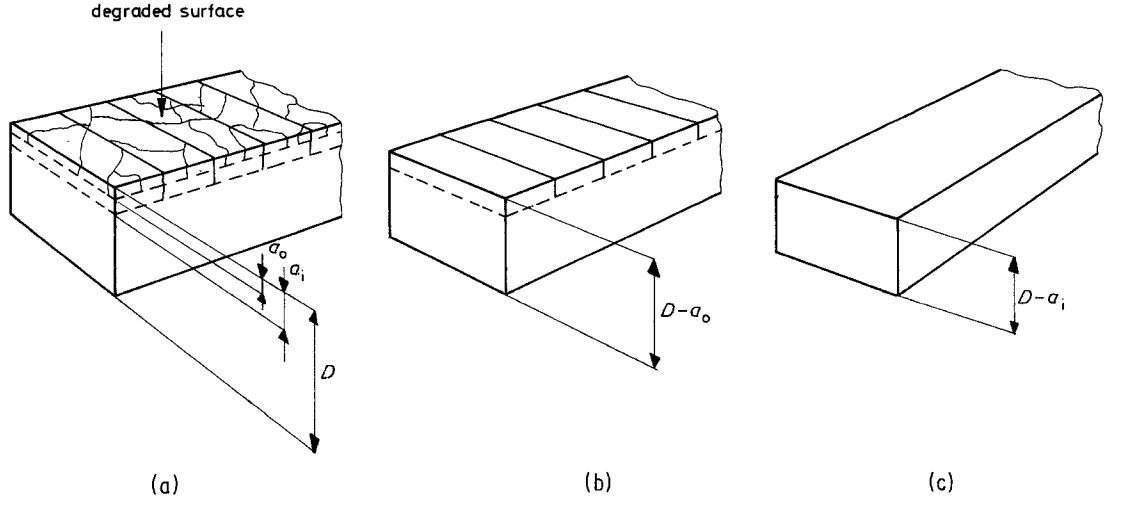

Figure 5 Measurement of the depth of a_0 and a_i. (a) Measurement of the entire depth of the specimen; (b) removal of the layer with randomly orientated cracks (if present), thickness measurement; (c) removal of the layer with perpendicular cracks, thickness measurement.

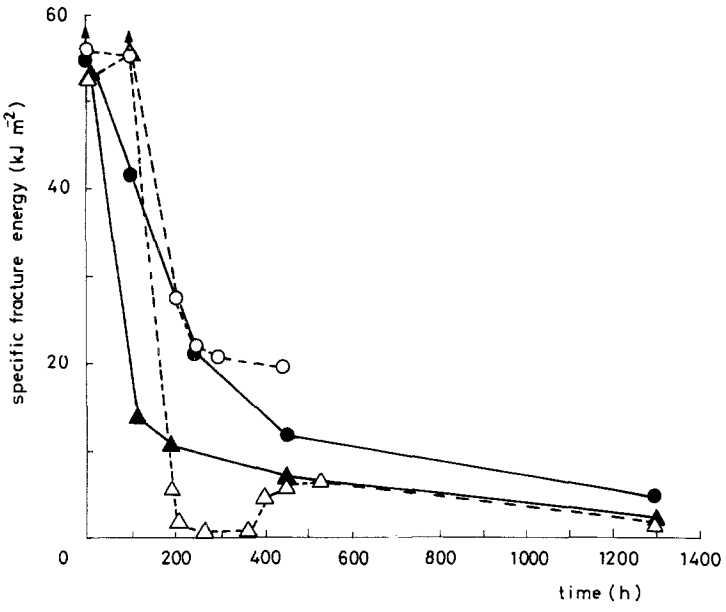

Figure 6 Specific fracture energy of degraded specimens compared to notched specimens. Material N (non-stabilized). Notch size equals degradation depth. (●) 0.01 m sec^{-1}, notched, (○) 0.01 m sec^{-1}, irradiated, (▲) 1.5 m sec^{-1}, notched, (△) 1.5 m sec^{-1}, irradiated.

deformation rates the data compare very well, while at 0.1 to 0.5 m sec^{-1} there is a transition. Data are scattered, some are in the range of the notched specimens, some are much lower. At 1.5 m sec^{-1} the specific fracture energy is definitely lower.

Fig. 8 shows the comparison for stabilized material. Here the overestimation of fracture resistance at 1.5 m sec^{-1} is less serious, but the underestimation at low speeds becomes worse.

5. Different fracture processes

The fracture processes that account for the results in the previous section are now described in more detail.

5.1. Crack arrest at interface

Correspondence between notched and degraded specimen data is expected if the embrittled layer fractures spontaneously during degradation, or somewhere at the beginning of the fracture process, and subsequently crack arrest occurs at the interface between the ductile and brittle material.

If we consider the situation in terms of an energy balance, crack arrest occurs in the case illustrated in Fig. 9. A small surface defect in the embrittled layer is supposed. As soon as $G > R$ at the crack tip (a_0), propagation will begin.

In a three-point bend specimen, G will increase with increasing crack length, even in fixed grip conditions (where the load decreases because of the increasing compliance). Thus more energy is supplied than is used up in creating new crack surfaces. The surplus energy is represented by the shaded area in Fig. 9. This increases crack speed, until the interface (a_i) is reached. From there crack propagation uses up more energy than that supplied, the crack will slow down and eventually arrest. G has to be increased and will be equal to that of a notched specimen at the moment crack propagation restarts. From Fig. 9 it is clear that crack arrest near a_i is promoted by a very brittle surface layer, or a large initial surface defect (a_0). In those cases, data of degraded and notched specimens will compare well.

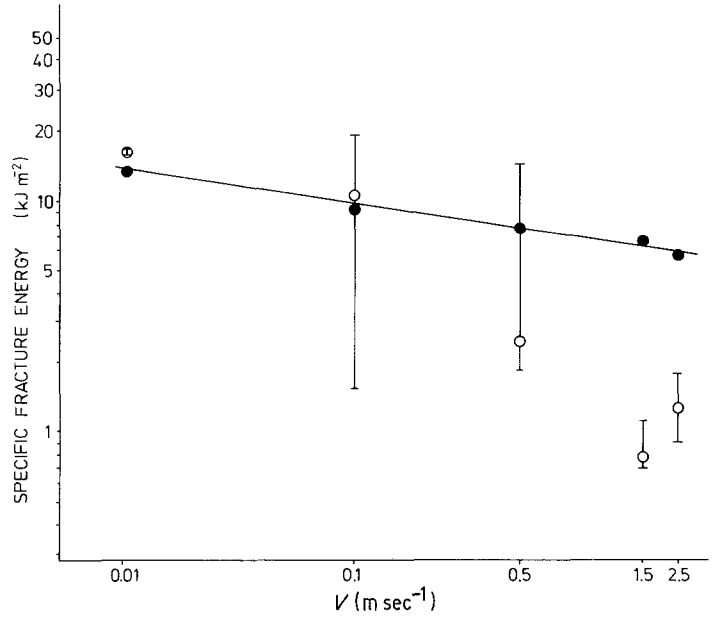

Figure 7 Specific fracture energy plotted against tup rate of specimens degraded for 250 h, and specimens with the corresponding notch size. Material N (non-stabilized). Vertical bar shows scatter-range. (●) Notched, (○) irradiated.

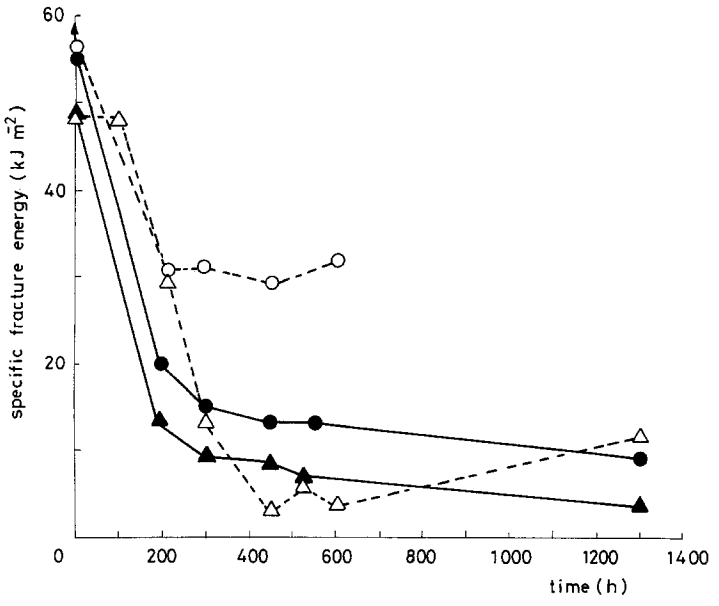

Figure 8 Specific fracture energy of degraded specimens compared with notched specimens. Material S (stabilized). (●) 0.01 m sec^{-1}, notched, (○) 0.01 m sec^{-1}, irradiated, (▲) 1.5 m sec^{-1}, notched, (△) 1.5 m sec^{-1}, irradiated.

5.2. Possibility of crack speed effects

Considering degraded specimens in three-point bending, the condition $G > R$ possibly remains fulfilled despite a rise in R at the interface (Fig. 10a). The fracture energy will be determined by the crack resistance of the embrittled material, but will never be lower than that of notched specimens.

However, in the material (N), for example, degraded for 250 h, the interface is sutuated at ~ 0.1 mm. It can be calculated from our results that G at the interface did not exceed 0.32 kJ m^{-2} while R was 1.46 kJ m^{-2} (tup rate 1.5 m sec^{-1}). The energy gained in front of the interface, is used up quickly behind it, and the crack should arrest. Apparently this does not occur.

It has previously been suggested by Rolland *et al.* [15] that this is caused by a crack speed effect. They argued that the increase of the fracture resistance at the interface between embrittled and ductile material will pass unnoticed because K_{id} brittle $> K_{Imin}$ ductile at the interface, where K_{id} brittle is the dynamical stress intensity of the embrittled material at the crack speed once the crack arrives at the interface, while K_{Imin} ductile is the minimum K_{id} value at which the ductile material achieves a steady state of continuing crack propagation.

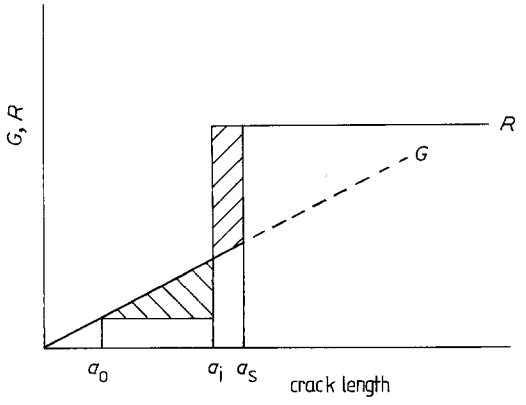

Figure 9 Conditions for crack arrest at the interface between embrittled and ductile material. a_i is degradation depth, a_0 is length of initial crack, a_s is the crack arrest point, G is energy release rate, R ($= G_c$) is crack resistance.

A simple analysis by Mott [16] showed that the crack speed during propagation will increase with the propagated distance

$$\dot{a} = \left(\frac{\pi}{k}\right)^{1/2} V_g[1 - (a/a_0)] \qquad (3)$$

and a limiting speed $(\pi/k)^{1/2} V_g$ will be reached. Here k is a constant and V_g is the speed of a longitudinal stress wave in the material.

Our findings prove that at the crack speed achieved at the interface, the crack is in some cases propagated although K is much smaller than K_{Ic} at crack initiation. Marshall and co-workers [17, 18] suggested that once the instability speed is reached, the fracture toughness of the material is reduced, possibly due to adiabatic conditions, causing heating. If at the interface, the crack has reached a speed higher than the instability speed of the tough material, the crack resistance is lowered due to thermal softening, and the crack will propagate anyhow. This is illustrated in Fig. 10b.

Another explanation for the lowering of the crack resistance at the tip of the running crack was suggested by So and Broutman [19]. They published results of tensile tests on high impact polystyrene (HIPS) coated with polystyrene (PS) and acrylonitrile–butadiene–styrene (ABS) coated with styrene acrylonitrile (SAN). They showed that a layer of the more brittle component of ~ 300 and 200 μm, respectively, on a 3 mm thick specimen of the ductile material was sufficient to cause brittle behaviour. This was attributed to the high crack speed at the interface which can be interpreted as a lowering of the test speed or rise of the glass transition temperature of the rubber particles in the ductile component, by the time–temperature equivalence principle. This renders the rubber particles ineffective as toughners.

We are at present studying the cause of the lowering of the fracture toughness at the interface in PP (by analysing the fracture paths, and varying test temperature).

5.3. Influence of spontaneous cracking

The previous analysis is based on one crack in the

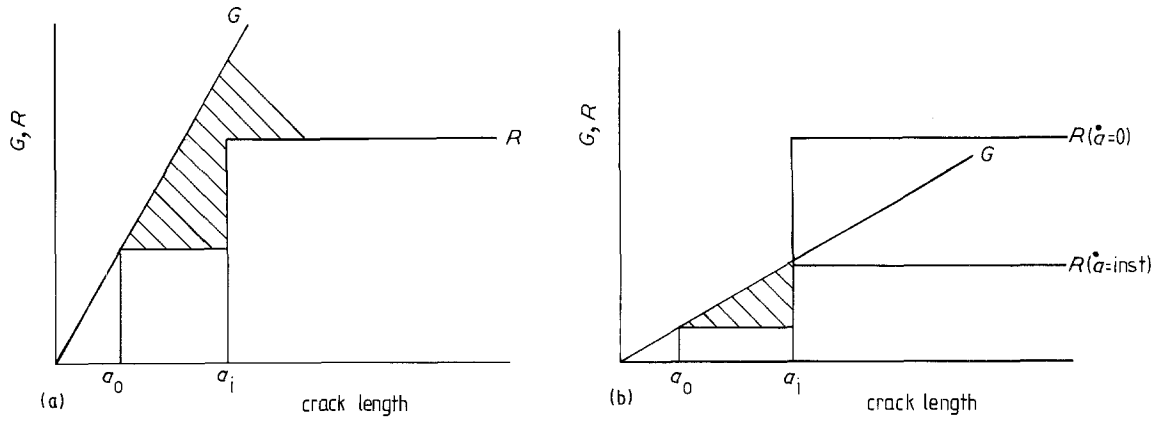

Figure 10 Continuing crack propagation (a) $G > R$ at the interface, (b) R reduced by crack speed.

entire specimen. After longer exposure times, the surface will crack spontaneously: a multitude of cracks develops. Because the surface layer will be very brittle at this stage, and the initial surface defects (a_0) are relatively large, the conditions are favourable for crack arrest. However, the fracture energy may be higher than that of notched specimens, because the cracks in the outer surface reduce the effective crack length. In extreme cases the specimen will behave as if the cracked layer is removed completely. This can be represented by shifting the origin in Fig. 9 to the right, resulting in higher G values for final fracture.

6. Fracture energy–degradation time relation

6.1. High tup rates

From Fig. 6 we conclude that different fracture mechanisms occur at different degradation times. The subsequent cases for non-stabilized PP at 1.5 m sec^{-1} are presented in Fig. 11. In the previous analysis, a homogeneously degraded layer is supposed. From Fig. 4 it is clear that this is not correct. The C=O index can be related to the number of chain scissions in PP [2] and thus to the molecular weight. It is known that for most polymers the fracture toughness decreases linearly with $1/\bar{M}_n$ [20], in a certain $\bar{M}_n$ (number average molecular weight) interval, but it is questionable how this relation will hold in the case of degradation localized in the amorphous zones [2]. It is clear, however, that the number of interlamellar tie molecules will decrease, causing embrittlement.

In Fig. 11 the R curves are smooth, which indicates that the increase in fracture resistance is not stepwise. At 100 h, the material is slightly degraded and no defects more serious than the inherent flaws that are present in the original material occur. Therefore, the

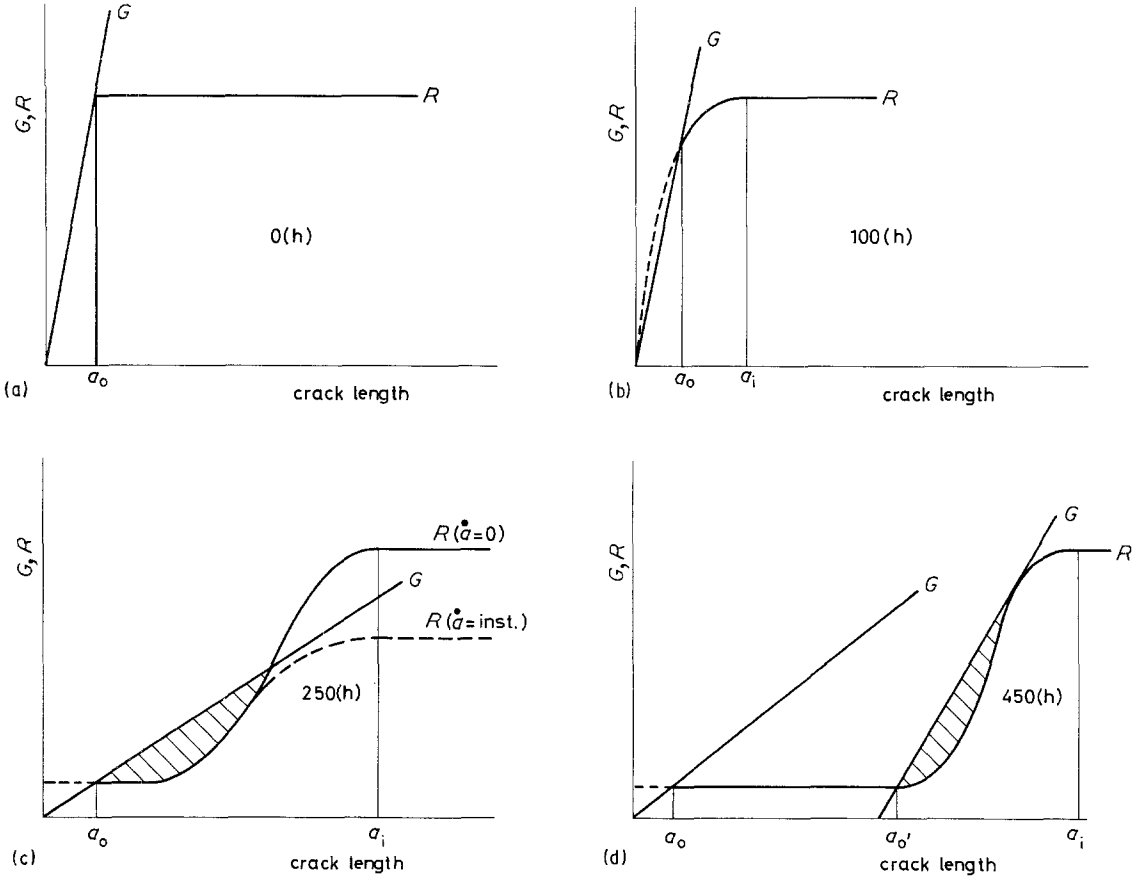

Figure 11 G and R curves for degradation times 0, 100, 250 and 450 h at 1.5 m sec^{-1}.

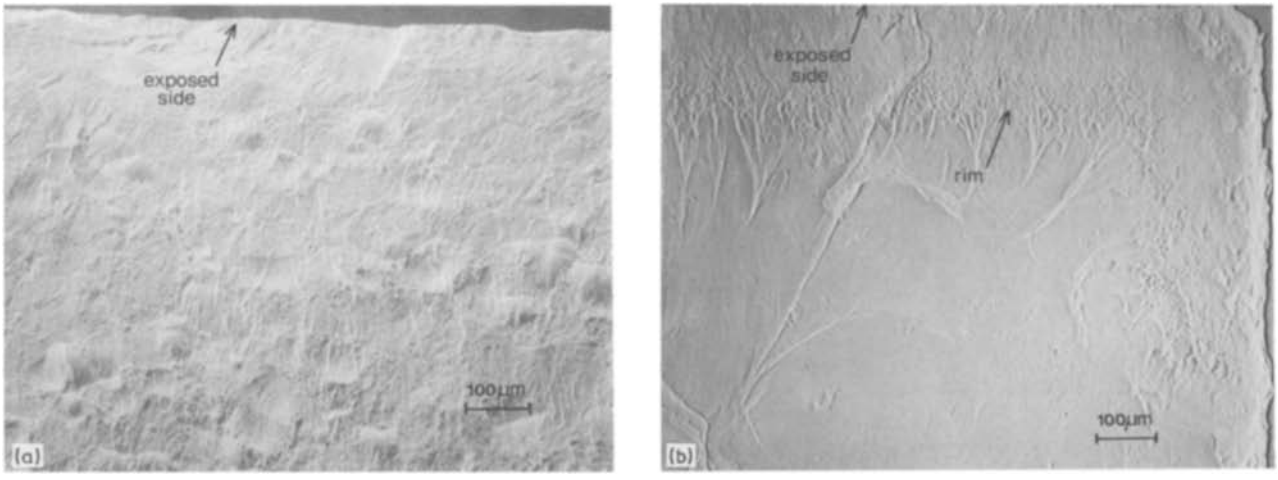

Figure 12 Scanning electron micrographs of fracture surfaces of specimens degraded for 300 h, (a) 1.5 m sec^{-1}, (b) 0.01 m sec^{-1}. Crack direction is from the top downwards.

fracture resistance about equals that at 0 h. At, for example, 250 h, a crack will initiate at some G value depending on the inherent flaw size and the brittleness of the surface material. Instability will follow caused by the crack speed effect.

The cracks forming next to the main crack (Fig. 3) do not affect the situation at the main crack's tip because they are in an earlier stage of growth and therefore shorter than the main crack. However, at 450 h, a dense pattern of cracks has grown spontaneously, and here the actual energy release rate at the main crack tip is lowered, which causes a rise in fracture energy (G').

The "peeling off" effect observed by other authors for PVC [21] and for PC [22] and which is suggested to cause regeneration of ductility [22] was not observed in the PP we examined. We did observe lumps of material breaking out of the surface. However, this occurred some time after the rise in fracture energy at 1.5 m sec^{-1} and cannot have been the cause of it. The peeling-off effect possibly does not occur in PP, or only at the much lower deformation rates applied in the publications mentioned [21, 22]. PP tested at low deformation rates [3] did not show the peeling-off effect either.

6.2. Fracture energy–degradation time relation at low tup rates

At 0.01 m sec^{-1} the embrittlement by the crack speed effect (Fig. 11c) is absent. Because the crack propagation speed is determined by the energy release, which apparently remains the same, this cannot simply be accounted for by the lower tup rate. Several hypotheses can be formed, explaining the more stable behaviour.

(a) The crack resistance of the embrittled material at initiation at low tup rates is lower [17], so the energy release is lower.

(b) The lower yield strength causes a larger plastic zone, which extends itself over the interface, into the ductile material. Its formation dissipates energy which is no longer available for crack speed increase.

(c) The lower yield strength in combination with the small specimen size, causes conditions between plane strain and plane stress, favouring stable crack propagation.

That the crack arrests at 0.01 m sec^{-1} is proved by Fig. 12. At 1.5 m sec^{-1} the fracture surface is completely smooth, while at 0.01 m sec^{-1} a distinct rim is visible. On closer inspection the rim shows a fibrillar structure indicating stable crack propagation.

Apparently, at 0.01 m sec^{-1} the crack has not reached the instability speed at the interface and arrests once the ductile material is encountered, after which it is reinitiated, and reaches instability under similar conditions as in the notched material.

The failure process at 0.01 m sec^{-1} is possibly a transition from the brittle behaviour above 0.5 m sec^{-1} to the ductile failure by "plastic fracture" described by Qayyum *et al.* [21] for PVC. The same dense population of surface cracks is observed but not the extensive ductility beneath the degraded layer. The ductility remains limited to crazing before the crack is reinitiated as shown in Fig. 12a. This is no doubt due to the much higher deformation rate in our test. We did not observe crack initiation from the centre, reported for extensively weathered PP in a slow uniaxial tension test [10].

At longer degradation times, the fracture energy is higher than that of the notched specimens at 0.01 m sec^{-1}, which is caused by the multitude of cracks formed during the fracture process. They do have an effect on the energy release rate here, because the process is stable. This is illustrated in Fig. 13 where the craze formation in front of one of these surface cracks is visible. This crack is formed during the fracture process and extends much deeper into the surface than when the specimen is fractured at higher tup rates.

6.3. Fracture energy–degradation time relation for stabilized material

The effect of the stabilizer is not yet completely clear. Degradation processes appear to slow down, and to be more confined to the surface. At 1.5 m sec^{-1} this promotes crack arrest. In fact, the points at 400 to 600 h are averages of scattered data. The fracture energies correspond to the fracture paths illustrated in Fig. 14. The forked path gives a high fracture energy,

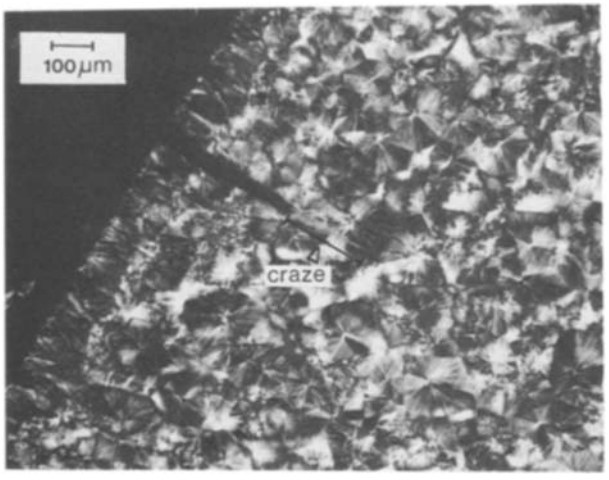

Figure 13 Microtomed slice in polarized light showing a surface crack in a specimen fractured at 0.01 m sec^{-1}.

comparing well with that of notched specimens, though usually somewhat higher (due to surface cracking). The forked path is also observed in notched specimens. The asymmetrical paths give lower fracture energies. The straight path occurs in the non-stabilized material, as a result of the crack speed effect (e.g. 250 h) but is occasionally also observed in the stabilized material.

Within the group of specimens fractured asymmetrically, there is a trend for higher fracture energies, when the crack starts further away from the centre. Besides that, on examination of the remaining parts, the larger part shows clear surface cracks perpendicular to the stress direction, from the centre up to the fracture. These are absent in the shorter specimen part. This indicates that there is competition between the crack arrest effect and the crack speed effect, which can be explained as follows.

During the deformation process, crack arrest occurs in the centre of the specimen. The deformation has to be increased until crack propagation restarts in the ductile material. This would cause a fracture with a high fracture energy and a forked path. Between the moment of crack arrest in the centre and the actual fracture, however, with increasing deformation, crack formation in the brittle layer spreads from the centre towards the sides. Apparently there are sites along the specimen length where the crack speed effect may occur. If these sites crack before the centre fractures, the crack will propagate due to the crack speed effect and an asymmetrical fracture is the result.

Sometimes such a site is present near the centre, and fracture energy will be low. In other specimens no such sites are present, and deformation has to be increased until the central crack restarts, and the fracture energy is high. The conclusion is that in the non-stabilized case, the crack speed effect acts over the entire specimen length, whereas in the stabilized case it only occurs on a limited number of sites.

The reduced chance of the occurrence of the crack speed effect is probably due to a lower difference $(a_i - a_0)$ in Equation 3. The degradation depth is somewhat smaller than in the non-stabilized material after the same degradation time (which does not show

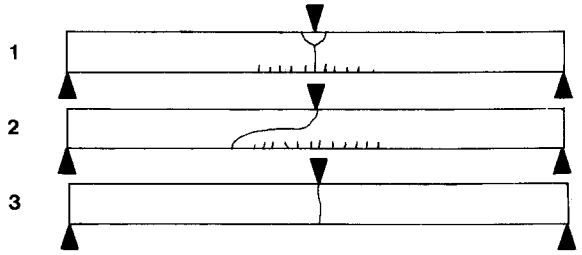

Figure 14 Fracture paths: (1) forked, (2) asymmetrical, (3) straight.

up in the comparison of the fracture energy in Figs 6 and 8 for notched material, because the stabilized material is initially more brittle). Furthermore, if a_i is large enough for the crack speed effect to occur, some small spontaneous defects are already present, preventing the crack speed effect.

It is interesting to compare this behaviour with that of non-stabilized material when it was precracked by fatigue. The specimens were fatigued in three-point bending. The intention was to prevent the crack speed effect by increasing a_0. The increase of a_0 was attained in the centre only, and this resulted in the same scattered results and fracture behaviour as in the stabilized material.

At 0.01 m sec^{-1} the specimen behaves as if the embrittled layer is almost completely removed, resulting in specific fracture energies that are much higher than that of the notched specimens. The smaller degradation depth compared to the non-stabilized material shows up here, in a much higher fracture energy.

7. Conclusions

The fracture energy is closely related to the condition of the embrittled layer. To predict the fracture energy quantitatively, the depth of embrittlement is not the only determining factor, however.

The simple theory, using defect size and fracture resistance to predict fracture resistance of degraded materials, overestimates the strength of the material at deformation rates over 0.5 m sec^{-1}, of non-stabilized PP for this specimen size and load geometry.

At the lower deformation rates, the results match better but the theory becomes increasingly conservative after longer exposure times, due to the spontaneous cracking of the surface.

For the stabilized material, data of degraded specimens are scattered at the higher deformation rates; however, in general, the model applies better. The underestimation of residual strength becomes unacceptable at lower deformation rates.

Further research should be aimed at establishing the conditions at which the crack speed effect occurs, and accounting for the effect of spontaneous surface cracking.

Acknowledgements

I would like to acknowledge the support of the following institutes: Plastics and Rubber Institute of TNO Netherlands (artificial degradation facilities and helpful discussion), Dutch State Mines (material preparation and artificial degradation facilities), Philips

PMF Netherlands (microtoming facilities) and the Materials Science Department of the Technical University of Delft (scanning electron micrographs).

References

1. B. RÅNBY and J. F. RABEK, "Photodegradation, Photo-oxidation and Photostabilisation of Polymers" (Wiley, London, 1975).
2. NORMAN S. ALLEN (ed.), "Degradation and Stabilisation of Polyolefins" (Applied Science, London, 1983) pp. 11–19.
3. E. KAY, A. DAVIS and G. L. PALMER, Conference on "The weathering behaviour of plastics and rubber" (PRI, Cambridge, 1976) lecture C2.
4. C. B. BUCKNALL and D. G. STREET, *J. Appl. Polym. Sci.* **12** (1968) 1311.
5. B. DOLEZEL, "Die Beständigkeit von Kunststof und Gummi" (Carl Hanser, Wien, 1978).
6. H. E. BAIR, D. J. BOYLE and P. G. KELLEHER, *Polym. Engng Sci.* **20** (1980) 995.
7. M. D. WOLKOWICZ and K. G. STATISH, *ibid.* **21** (1981) 571.
8. M. G. WYZGOSKI, *J. Appl. Polym. Sci.* **26** (1981) 1689.
9. K. BERGER, Lecture at the "Hanauer Symposium: Beschleunigte Prufung der Licht und Wetterbeständigkeit von Kunststoffen und Lacken" (October, 1975).
10. M. M. QAYYUM and J. R. WHITE, *J. Mater. Sci.* **21** (1986) 2391.
11. A. V. CUNLIFFE and A. DAVIS, *Polym. Deg. Stab.* **4** (1982) 17.
12. E. PLATI and J. G. WILLIAMS, *Polym. Engng Sci.* **15** (1975) 470.
13. A. SANDT, *Kunststoffe* **12** (1982) 791.
14. T. CASIRAGHI and A. SAVADORI, *Plastics Rubber, Mater. Appl.* **2** (1980) 1.
15. L. ROLLAND, K. THOMSON, S. MOSTOVOY and L. BROUTMAN, Conference on "Deformation, Yield and Fracture of Polymers" (PRI, Cambridge, 1982) lecture II.
16. N. F. MOTT, *Engineering* **165** (1948) 16.
17. G. P. MARSHALL, L. H. COUTS and J. G. WILLIAMS, *J. Mater. Sci.* **9** (1974) 1409.
18. J. G. WILLIAMS, "Fracture Mechanics of Polymers" (Wiley, Chichester, 1984) p. 157.
19. P. SO and L. J. BROUTMAN, *Polym. Engng Sci.* **22** (1982) 888.
20. P. I. VINCENT, *Polymer* **1** (1960) 425.
21. M. M. QAYYUM and J. R. WHITE, *Polymer* **28** (1987) 469.
22. E. S. SHERMAN, A. RAM and S. KENIG, *Polym. Engng Sci.* **22** (1982) 457.

Received 23 April
and accepted 22 September 1987